ISSN 1693-4393

CFD Simulation and Efficiency Analysis of Natural Gas Ejector-Booster System

Aditya Kurniawan[1*], Rafida Nariswari Nuzuladzmi[1], Amanda Lailia Nur Afni[1]

[1]Program Studi Teknik Kimia, FTI, UPN "Veteran" Yogyakarta

[*]*E-mail*: aditya.kurniawan@upnyk.ac.id

Abstract

Natural gas production involving several gas-well streams with different operating pressure creates a problem, especially for lower-pressure streams. Usually, a compressor unit is installed to enable a lower-pressure stream to tie in the higher-pressure stream. However, this solution requires high costs and investment related to compressor operation. Natural gas ejector provides an alternative, where a higher-pressure stream act as the motive fluid to withdraw the lower-pressure stream. This work aims to simulate the flow inside the ejector using ANSYS Fluent CFD simulator. The model used is validated to published data by other authors. Ejector efficiency is calculated for several operating pressure and ejector geometry: ratio of mixing tube length to diameter. We found that the variation in L/D ratio of mixing tube in current study did not significantly affect the ejector performance. Conversely, it was strongly affected by both motive and suction pressure, where the entrainment ratio is generally higher for lower pressure ratio. On the other hand, the efficiency of ejector process exhibited an optimum behavior, where we obtained the highest efficiency of 26.7% at pressure ratio of 0.1765. Therefore, this result can be utilized as the recommended operating condition.

Keywords: *natural gas; ejector; efficiency; CFD; simulation*

Introduction

The technology of gas ejectors has been successfully implemented to recover low-pressure gas from flare gas systems. It also has been applied to boost production from low-pressure natural gas well, especially in the presence of higher-pressure gas source nearby (Ping & Brian, 2020). A gas ejector is a compression equipment whose operation is based on Bernoulli Principle. It generates a vacuum effect from the conversion of high-pressure gas flow (motive gas) into high velocity through a nozzle. Lower-pressure (suction) gas is then absorbed by the vacuum and mixed with high-velocity flow as displayed in Figure 1(a). The pressure is then recovered by a diffuser to an intermediate (discharge) pressure (transvac, 2022). The ejector system consists of three main parts, i.e., nozzle, mixing chamber, and diffuser as shown in Figure 1(b).

The evaluation of ejector performance involves key parameters like the mass entrainment ratio, pressure ratio, and ejector efficiency (Chong et al., 2009; Liu, 2014). Ejector performance can be optimized by adjusting the operating condition, fluid selection, and geometry of ejector parts. Ruangtrakoon et al., (2011) investigate the effect of the motive-gas nozzle on ejector performance. They apply several throat diameters which result in different Mach Numbers. The sudden reduction of the Mach Number is caused by the reverse flow in the mixing chamber. Therefore the distance between the nozzle exit and mixing chamber entrance (NXP) affects the mass entrainment from suction flow (Aldas et al., 2013). Vu & Kracik, (2018) mention that the mass entrainment ratio is related to the change of turbulence kinetic energy inside the ejector. Kracik & Dvorak, (2017) and Setyono et al., (2022) showed that the exit position of the nozzle (NXP) has a lesser effect on the optimal value of the entrainment ratio than the ratio of diameter-to-length (R) of the mixing chamber shows a significant effect. Other geometrical parameter such as the angle of secondary nozzle is insignificant toward ejector performance (Chong et al., 2009). Pressure ratio between motive and suction flow is proportionally related with entrainment ratio, however after certain point it become less significant. Also there is a minimum motive pressure necessary to enable gas from lower pressure nozzle enter the mixing chamber (Setyono et al., 2022).

The ejector efficiency is largely affecting the performance of overall gas ejector-booster system. However, the works that focused on ejector efficiency is still limited (Liu, 2014). This work aims to analyze the performance of natural gas ejector, especially from the efficiency aspect. A CFD model is constructed and validated to measurement data from previous works. Several variations in ejector geometry and operating are employed to analyze the effect of each variable toward the ejector efficiency.

ISSN 1693-4393

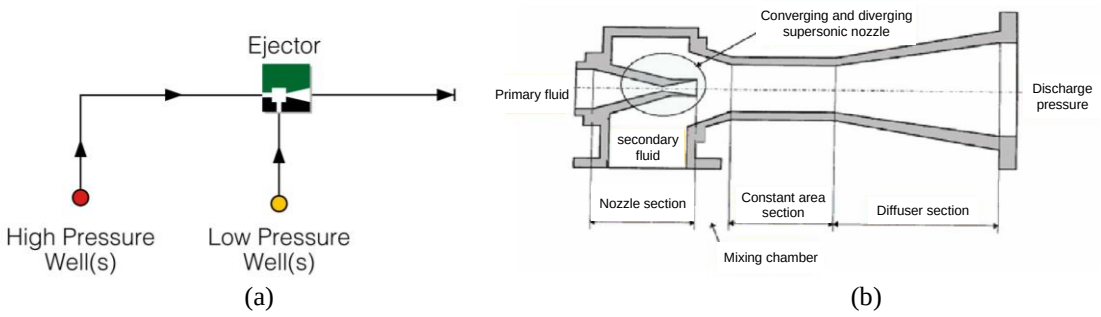

Figure 1. (a) Schematic of natural gas ejector-booster system to increase production from low pressure gas well (b) components of gas ejector (Source: Ping & Brian, 2020; transvac, 2022)

Methods

This study is performed by developing a computational fluid dynamics (CFD) model and simulate the ejector compression process of natural gas. Methane is the most dominant component of natural gas. Therefore, we use methane gas as the reference for natural gas properties. The steps performed in this study is explained in Figure 2 and Figure 3.

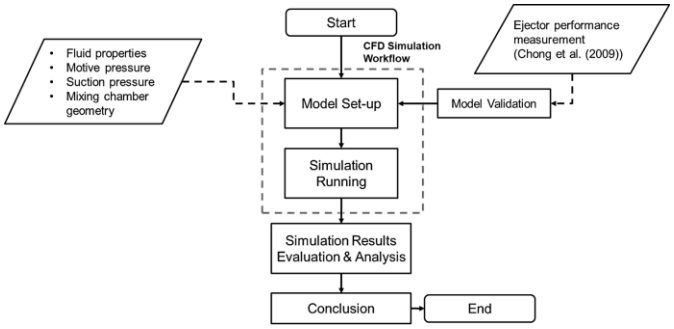

Figure 2. Flowchart of current study

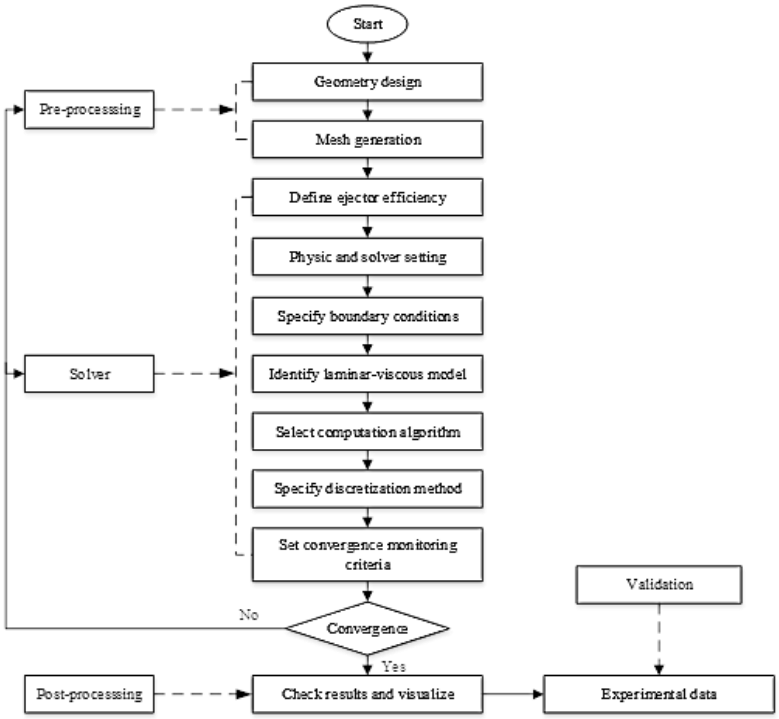

Figure 3. Flowchart of CFD simulation

ISSN 1693-4393

The set of ejector geometry and independent variables used for this study refers to the work by Setyono et al., (2022), as shown in Table 1 and Figure 4. However, we made several modifications to the variable set. First, for the pressure of motive fluid, we only considered 3 variables because the study indicated that the optimum variable falls within that range. For the pressure of suction fluid, we put additional points since previous study did not investigate the variation of suction pressure.

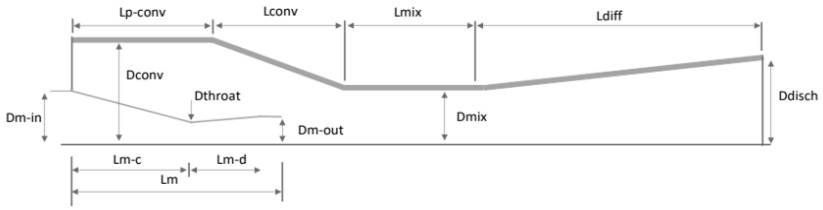

Symbols	Parameters	Value (mm)
Dm-in	Diameter Motive Inlet	50
Dm-out	Diameter Motive Inlet	22
Dthroat	Diameter Motive Inlet	13
Lm	Length of Motive	200
Lm-c	Length Motive Converging	120
Lm-d	Length Motive Diverging	60
Dconv	Diameter Converging	90
Dmix	Diameter Mixing Tube	29
Ddisch	Diameter Discharge	80
Lmix	Length Mixing Tube	100
Lp-conv	Length Pre Converging	150
Lconv	Length Converging	130
Ldiff	Length Diffuser	300

Figure 4. Ejector geometry specification (Setyono et al., 2022)

Table 1. Set of independent and controlled variables

P_m (psig)	P_s (psig)	P_d (psig)	(L/D_{mix})
220	10	50	3.31
240	20	50	3.44
260	30	50	3.57

In order to assess the ejector performance, we calculate two key variables, i.e. the mass entrainment ratio and the ejector efficiency. The mass entrainment ratio (φ) and ejector efficiency (η) is defined by the following equation (Liu, 2014):

$$\varphi = \frac{\dot{m}_s}{\dot{m}_m}; \qquad \eta = \varphi \frac{(h'_{s,isen} - h_s)}{(h_m - h'_{m,isen})}$$

The mass entrainment ratio is obtained from simulation result, while the enthalpy is read from methane P-H diagram (Kidnay et al., 2019)

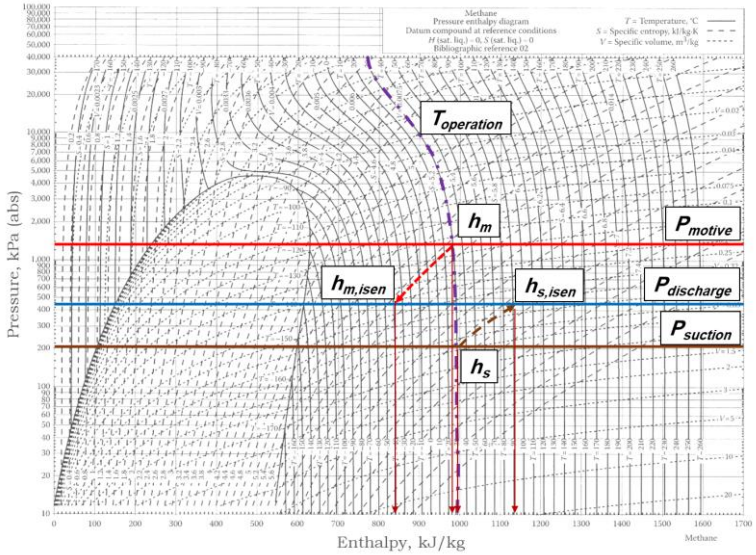

Figure 5. Methane P-H diagram (Kidnay et al, 2019)

ISSN 1693-4393

CFD Modeling and Simulation

CFD is a mathematical modeling method that solves the continuity and flow equations (momentum conservation), as well as other corresponding equation, depending on the modeling scope of a study. The flow equation utilized here is the Navier-Stokes equation, which is treated by Reynolds averaging to accommodate the turbulence in the flow. The equation takes the following form.

$$\frac{\partial}{\partial t}(\rho \boldsymbol{u_i}) + \frac{\partial}{\partial x_j}(\rho \boldsymbol{u_i u_j}) = -\frac{\partial p}{\partial x_i} + \frac{\partial}{\partial x_j}\left[\mu\left(\frac{\partial \boldsymbol{u_i}}{\partial x_j} + \frac{\partial \boldsymbol{u_j}}{\partial x_i} - \frac{2}{3}\delta_{ij}\frac{\partial \boldsymbol{u_l}}{\partial x_l}\right)\right] + \frac{\partial}{\partial x_j}\left(-\rho\overline{u_i' u_j'}\right)$$

The last term in the right side of equation is called Reynolds stress that emerges from the fluctuation due to turbulence. To calculate the Reynolds stress, a Boussinesq hypothesis is applied by following equation

$$-\rho\overline{u_i' u_j'} = \mu_t\left(\frac{\partial \boldsymbol{u_i}}{\partial x_j} + \frac{\partial \boldsymbol{u_j}}{\partial x_i}\right) - \frac{2}{3}\left(\rho k + \mu_t \frac{\partial \boldsymbol{u_k}}{\partial x_k}\right)\delta_{ij}$$

To calculate the turbulence viscosity, μ_t, several approach can be implemented and it determines the turbulence model.

We use Ansys 2022 R2 student license for running the simulation workflow. The ejector geometry is represented using 2D axisymmetric type, illustrated in Figure 6. To establish the appropriate number of cells, we conduct grid sensitivity analysis by comparing simulation result for varying number of grid cell. Figure 7 displays the analysis result, and based on them, we selected 73,979 as optimal number of grid cells. This decision is justified by the insignificant difference in simulation results for larger grid number, allowing us to maintain accuracy while minimizing computational load.

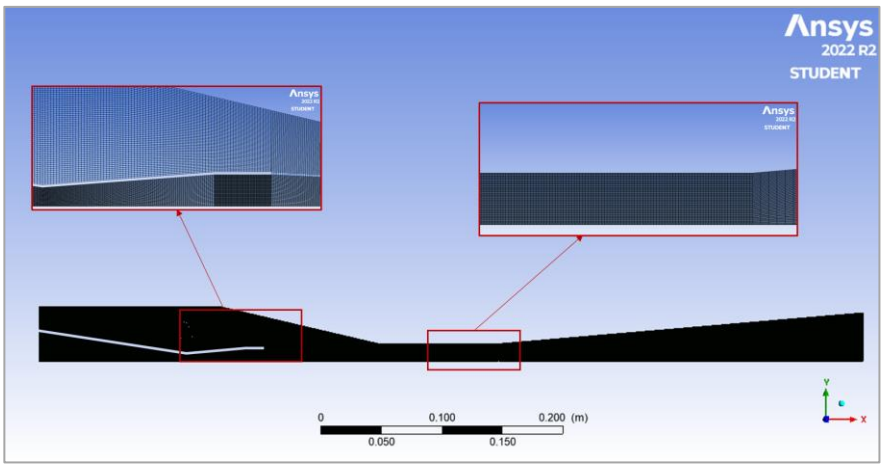

Figure 6. Geometry modelling and meshing

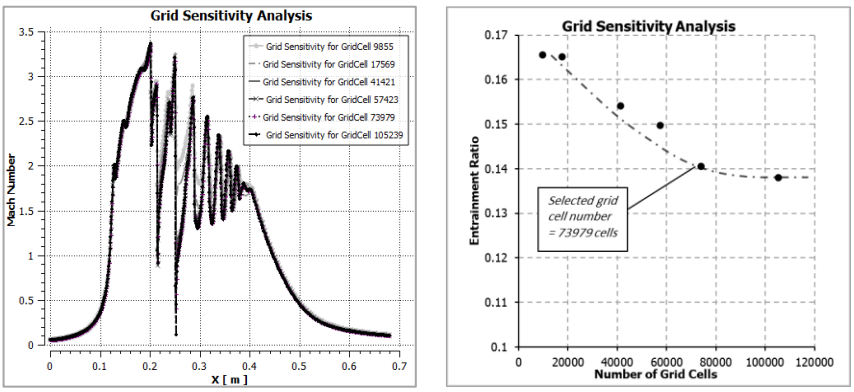

Figure 7. Grid Sensitivity Analysis

The natural gas is modeled as CH_4 (methane). The specification for fluid model is shown in Table 2. For this study, we refer to Setyono et al., (2022) for the gas model selection. For thermal properties, we assume the constant value for both heat capacity and thermal conductivity because the low system temperature, with temperature of both

ISSN 1693-4393

inlet stream are 300 K. Whereas for viscosity, based on literature data for methane, we put the formula of viscosity as a function of pressure into the simulator.

Table 2. Fluid material specification

Parameter	Remarks
Materials	Methane (CH_4)
Density	Ideal gas model
Heat capacity	2222 J/kg.K
Thermal conductivity	0.0332 W/mK
Viscosity (pressure dependent)	$(5.586x10^{-13}*P\ [Pa] + 9.185x10^{-6})$ kg/m s
Molecular weight	16.04303 kg/kmol

Due to the nature of high velocity compressible flow in the ejector, we selected the density-based solver, so that it can be modeled more accurately. To model the turbulence, RNG k-ε model is used, therefore to calculate the turbulence viscosity, two additional transport equations that involve both variables, k and ε, are added and solved simultaneously. Also, we implement the compressibility effects to the flow equation. We set the pressure inlet and pressure outlet boundary condition for each flow in and flow out of the ejector. For the initialization, hybrid initialization option is used to obtain better initial guess for the simulation. The settings of density-based solver are: formulation: implicit; flux scheme: AUSM; and solution steering flow type: transonic.

Results and Discussions

The CFD model constructed for this study is validated using the ejector operation data measured by Chong et al., (2009). The data is selected based on the similarity of fluid used in their study. The validation results are presented in Figure 8, where the entrainment ratio is compared between the measurement and simulation. From three points, all the simulation is located within the 10% error line.

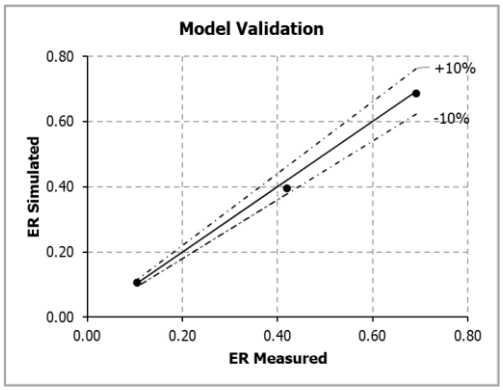

Figure 8. Model Validation

The CFD simulation was initially conducted using the given range of variables. However, for the suction pressure of 20 and 30 psi, the maximum entrainment ratio is not achieved. Therefore, we put additional motive pressure (180 psi and 200 psi) for both suction pressure value and we got the result that give a maximum entrainment ratio as shown in Figure 9, Figure 14 and Figure 15.

Based on the result in Figure 9, it was observed that the variation of mixing tube geometry within the range investigated in this work, did not have significant impact the ejector's performance. This results differ from previous study conducted by Setyono et al., (2022), where an increase of L/D ratio of mixing tube from 3.44 to 3.57 resulted in a substantially lower entrainment ratio. Falsafioon et al., (2019) pointed out the role of internal flow configuration inside the mixing chamber toward ejector performance, and for three L/D ratio of mixing tube the flow structure of is not significantly varied, as displayed in Figure 10. The separation between sonic and subsonic flow is expressed by bold contour of Mach number = 1, plotted in the figure. The form of the contour in the mixing chamber and mixing tube is quite similar. Chong et al., (2009) and Hassan Amin et al., (2019) both identify that the L/D ratio affects proportionally toward the entrainment ratio until some optimum value, where further increase of L/D ratio do not improve the entrainment ratio significantly. It is likely that the range of L/D ratio utilized in this study has already exceeded the optimum value; hence; the deviation of ejector performance is not significant.

For each suction pressure value, we found a different optimum motive pressure. This trend align with the experimental result by Chong et al., (2009) where the entrainment ratio initially increases with motive pressure, then

ISSN 1693-4393

for certain optimum value the trend is reversed. This behavior is related with the flow conditions generated by the motive stream as it pass through primary nozzle, whether it is under-expanded, ideally-expanded, or over-expanded.

When the flow condition is ideally-expanded, the pressure at the exit of primary nozzle approaches the suction pressure and it becomes ideal condition, where double-choking flow is generated inside the mixing chamber. For over-expanded condition, the pressure of motive stream at the nozzle exit is lower than suction pressure, and in this condition, shockwave is created and thus created an energy loss by motive stream. Conversely, the under-expanded condition indicate that the energy provided by the motive stream is insufficient, leading to poor creation of double-choking condition in the mixing chamber, therefore it lowers the suction flow rate and also the entrainment ratio.

The conditions above can be examined in Figure 11 and Figure 12. The motive pressure of 200 psig gives the highest entrainment ratio (0.567) where we can analyze that the sonic line approaches the mixing tube wall, therefore the double-choking flow is occurred. Moreover, from the pressure profile, the pressure at nozzle exit approaches the suction pressure. For higher motive pressure (220 psig), the flow become over-expanded and therefore the shockwave created will reduce the energy of motive stream when enter the mixing chamber, even if the double-choking condition is created in mixing tube. For a lower motive pressure (180 psig), the sonic region is poorly established in the mixing chamber, and therefore the flow might enter the single-choking region, even if the pressure at the nozzle exit is almost similar to suction pressure.

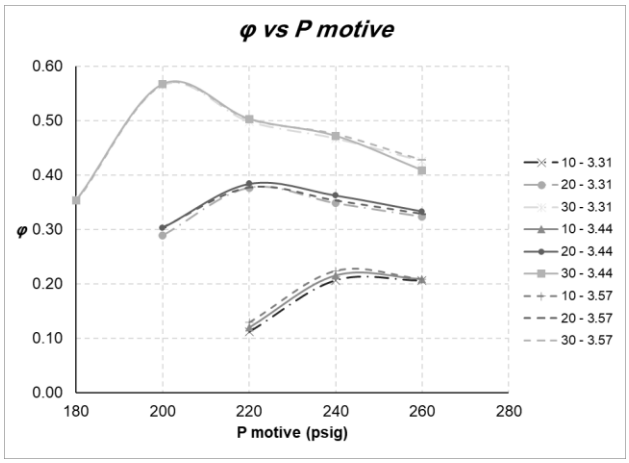

Figure 9. Entrainment ratio vs motive pressure for different geometry and suction pressure

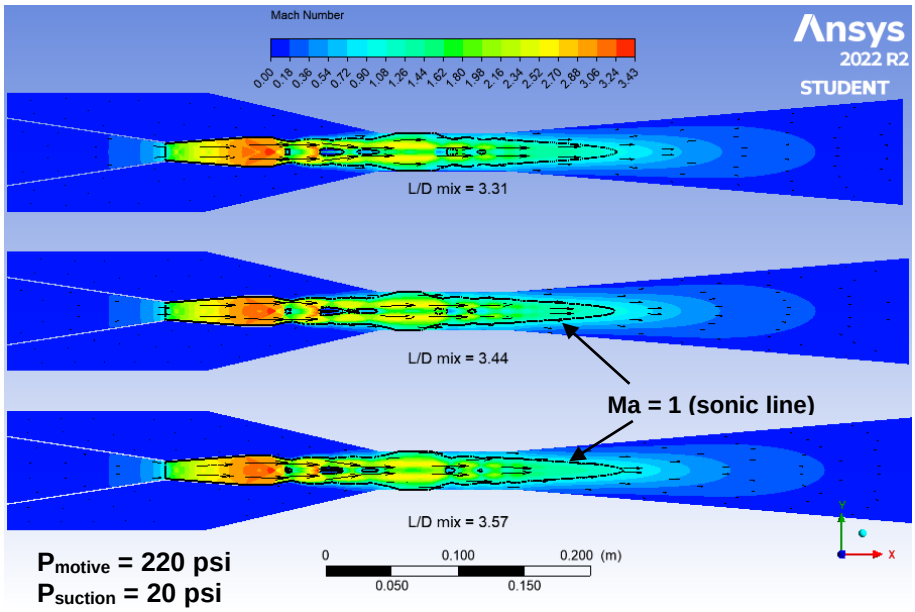

Figure 10. Velocity profile for each different L/D ratio of mixing tube

ISSN 1693-4393

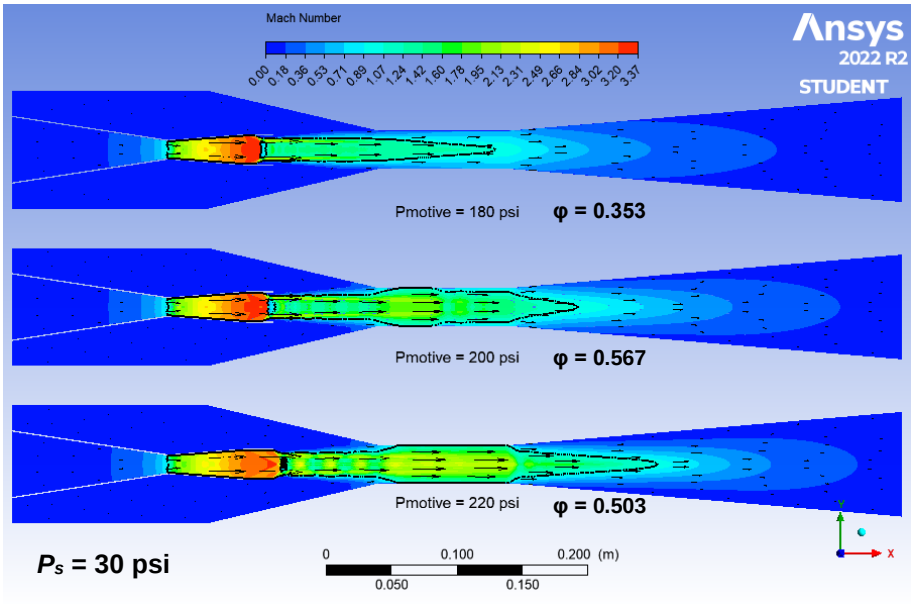

Figure 11. Velocity distribution for different motive pressure

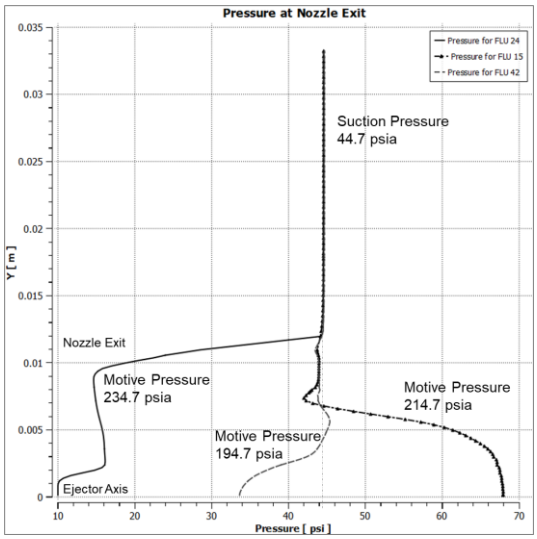

Figure 12. Pressure profile at nozzle exit for different motive pressure

For the variation in suction pressure, we observe that increasing the suction pressure improves the entrainment ratio. This finding is supported by the velocity distribution depicted in Figure 13, where a higher suction pressure gives a more favorable profile of sonic flow inside the mixing chamber. Similar with the variation of motive pressure, the contour of sonic flow closer to mixing tube wall for higher suction pressure. This facilitates the formation of double-choking flow, thereby increasing the entrainment of the suction stream.

To accommodate the influence of both motive and suction pressure, we implemented the pressure ratio that is defined by Chong et al., (2009) in their work. In general, the relationship between the entrainment ratio and the pressure ratio demonstrated the inverse proportionality, as illustrated in Figure 14. This result confirms the previous finding reported by Chong et al., (2009). However, the maximum entrainment ratio achieved in the current study is comparatively lower due to the different ejector geometry and variable setup employed, which may have contributed to variations in the results.

ISSN 1693-4393

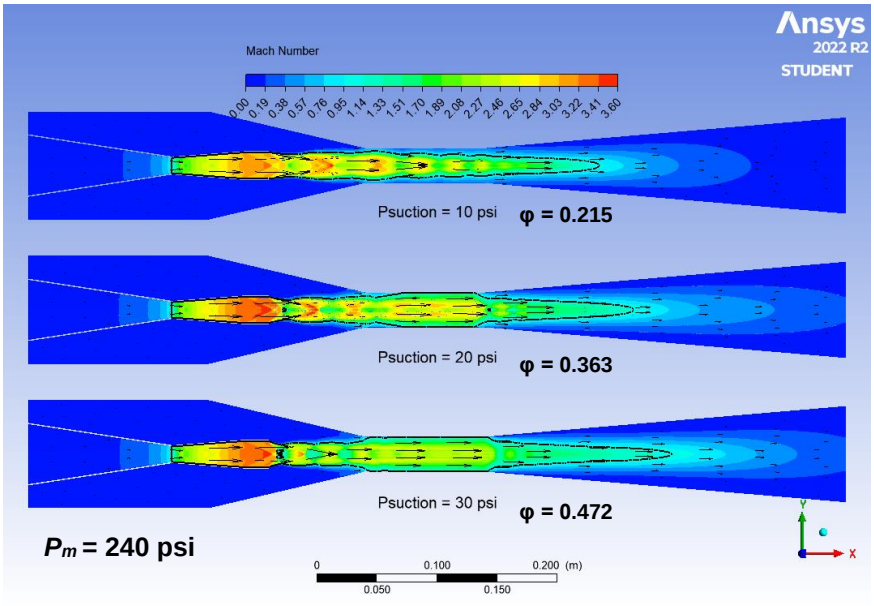

Figure 13. Velocity distributions for different suction pressure

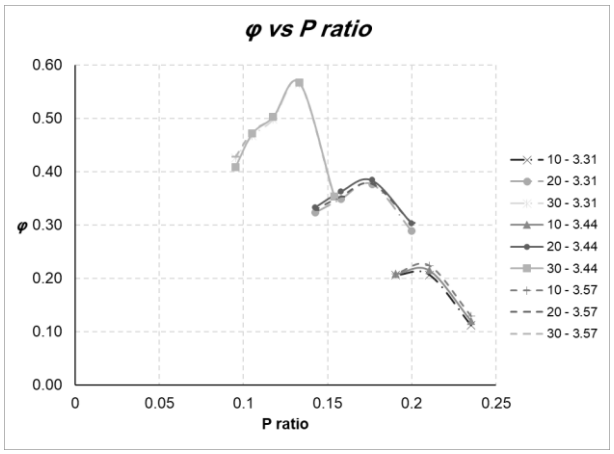

Figure 14. Entrainment Ratio vs Pressure Ratio

Based on above result, the higher entrainment ratio can be achieved by utilizing low pressure ratio. This is linked with higher motive and suction pressure. A higher motive pressure means larger energy input for the ejector process. On the contrary, higher suction pressure results in lower pressure gain achieved through ejector operations. Consequently, it is crucial to analyze the efficiency of the ejector operation, especially related with the setting of motive and suction pressure.

The profile of ejector efficiency toward the pressure ratio is presented in Figure 15. Based on the range of independent variables, we identified an optimum profile in terms of the pressure ratio, achieving the highest efficiency of 26.7% at a pressure ratio of 0.1765. This optimal condition corresponds to a motive pressure of 220 psig and a suction pressure of 20 psig. It should be noted that a higher suction pressure (30 psig) results in a lower pressure ratio and thus higher entrainment ratio, but the process become less efficient due to the lower pressure gain in the suction stream. The decrease in efficiency also observed in higher pressure ratio, mainly due to the reduced entrainment ratio. The operating condition that is pointed out by arrow in Figure 15 is associated with the motive pressure of 180 psig and suction pressure of 30 psig. During the simulation, we found oscillation in the iteration result, therefore we suspect that might be there is an error in the entrainment ratio, and therefore the efficiency is deviated from the trend. Eventually, there is a range of pressure ratio that is correlated to efficient ejector operation, so that it can be utilized as the recommended operating condition.

ISSN 1693-4393

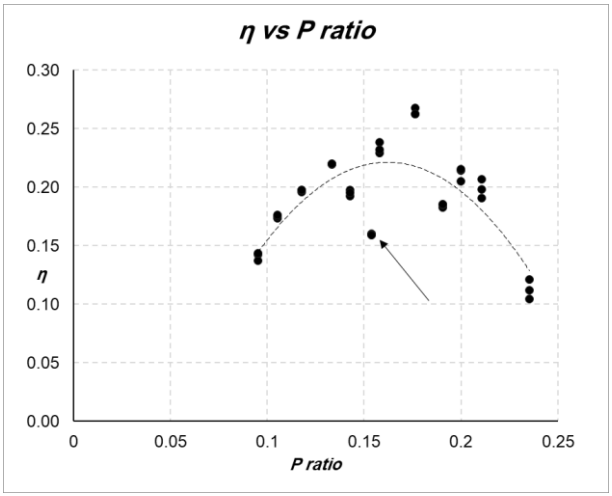

Figure 15. Ejector Efficiency vs Pressure Ratio

Conclusions

A CFD model of a natural gas ejector-booster was constructed and validated toward data from previous study. It was observed that within the range of L/D ratio of mixing tube applied in current study, the ejector performance is not significantly difference. However, its performance is strongly affected by both motive and suction pressure, where the entrainment ratio is generally higher for lower pressure ratio. On the other hand, the efficiency of ejector process exhibited an optimum behavior, where we achieved highest efficiency at 26.7% at pressure ratio of 0.1765. Therefore, this result can be utilized as the recommended operating condition.

Acknowledgement

We would like to express our gratitude to ANSYS for providing the student license for their software bundle that was utilized in this study.

List of Symbols

φ = mass entrainment ratio [fraction]
$\dot{m}_m$ = mass flow rate of motive stream [kg/s]
$\dot{m}_s$ = mass flow rate of suction stream [kg/s]
η = ejector efficiency [percent] $= \varphi \frac{(h'_{s,isen} - h_s)}{(h_m - h'_{m,isen})}$
h_m = specific enthalpy of motive stream [kJ/kg]
h_s = specific enthalpy of motive stream [kJ/kg]
$h'_{m,isen}$ = specific enthalpy of isentropic expansion of motive stream [kJ/kg]
$h'_{s,isen}$ = specific enthalpy of isentropic compression of suction stream [kJ/kg]
P_m = motive pressure [psia]
P_s = suction pressure [psia]
P_d = discharge pressure [psia]
P_{ratio} = pressure ratio [dimensionless] $= \frac{P_d - P_s}{P_m - P_d}$

References

Aldas, K., Sen, F., & Ozkul, I. (2013). The Investigation of Gas Ejector Performance using CFD Modelling. *TEM Journal*, *2*(2), 130–135.

Chong, D., Yan, J., Wu, G., & Liu, J. (2009). Structural optimization and experimental investigation of supersonic ejectors for boosting low pressure natural gas. *Applied Thermal Engineering*, *29*(14–15), 2799–2807. https://doi.org/10.1016/j.applthermaleng.2009.01.014

Falsafioon, M., Aidoun, Z., & Ameur, K. (2019). Numerical Investigation on the Effects of Internal Flow Structure on Ejector Performance. *Journal of Applied Fluid Mechanics*, *12*(6), 2003–2015. https://doi.org/10.29252/jafm.12.06.29895

Hassan Amin, A., Elbadawy, I., Elgendy, E., & Fatouh, M. (2019). Effect of geometrical factors interactions on design optimization process of a natural gas ejector. *Advances in Mechanical Engineering*, *11*(9),

ISSN 1693-4393

168781401988036. https://doi.org/10.1177/1687814019880368

Kidnay, A. J., Parrish, W. R., & McCartney, D. G. (2019). Appendix B. In *Fundamentals of Natural Gas Processing* (Third). CRC Press.

Kracik, J., & Dvorak, V. (2017). Preliminary study of the primary nozzle position of a supersonic air ejector with a constant-area mixing chamber. *EPJ Web of Conferences*, *143*, 02056. https://doi.org/10.1051/epjconf/201714302056

Liu, F. (2014). Review on Ejector Efficiencies in Various Ejector Systems. In *15th International Refrigeration and Air Conditioning Conference*. Purdue: School of Mechanical Engineering, Purdue University.

Ping, W., & Brian, M. (2020). Giving a Boost to Low Pressure Gas Well by Installing Gas Ejector. In *Day 2 Wed, October 30, 2019*. SPE. https://doi.org/10.2118/196440-MS

Ruangtrakoon, N., Aphornratana, S., & Sriveerakul, T. (2011). Experimental studies of a steam jet refrigeration cycle: Effect of the primary nozzle geometries to system performance. *Experimental Thermal and Fluid Science*, *35*(4), 676–683. https://doi.org/10.1016/j.expthermflusci.2011.01.001

Setyono, A. E., Utomo, M. S. . T. S., & Aminata, J. (2022). Numerical Analysis of Geometry Ejector for Boosting Low Pressure Natural Gas. *International Journal of Engineering Research & Technology (IJERT)*, *11*(6), 266–269.

transvac. (2022). Ejectors for the Oil & Gas Industry. May 10, 2023, https://www.transvac.co.uk/wp-content/uploads/Transvac-Ejectors-Oil-Gas-Solutions-Small.pdf

Vu, N. Van, & Kracik, J. (2018). CFD simulation of ejector: is it worth to use real gas models? *EPJ Web of Conferences*, *180*, 02075. https://doi.org/10.1051/epjconf/201818002075